Dephasing enhanced transport in nonequilibrium strongly correlated quantum systems

J. J. Mendoza-Arenas,[1] T. Grujic,[1] D. Jaksch,[1,2] and S. R. Clark[1,2]
[1]*Clarendon Laboratory, University of Oxford, Parks Road, Oxford OX1 3PU, United Kingdom*
[2]*Centre for Quantum Technologies, National University of Singapore, 3 Science Drive 2, 117543 Singapore*
(Received 22 February 2013; revised manuscript received 22 May 2013; published 24 June 2013)

A key insight from recent studies is that noise, such as dephasing, can improve the efficiency of quantum transport by suppressing coherent single-particle interference effects. However, it is not yet clear whether dephasing can enhance transport in an interacting many-body system. Here, we address this question by analyzing the transport properties of a boundary driven spinless fermion chain with nearest-neighbor interactions subject to bulk dephasing. The many-body nonequilibrium stationary state is determined using large-scale matrix product simulations of the corresponding quantum master equation. We find dephasing enhanced transport only in the strongly interacting regime, where it is shown to induce incoherent transitions bridging the gap between bound dark states and bands of mobile eigenstates. The generic nature of the transport enhancement is illustrated by a simple toy model, which contains the basic elements required for its emergence. Surprisingly, the effect is significant even in the linear response regime of the full system, and it is predicted to exist for any large and finite chain. The response of the system to dephasing also establishes a signature of an underlying nonequilibrium phase transition between regimes of transport degradation and enhancement. The existence of this transition is shown not to depend on the integrability of the model considered. As a result, dephasing enhanced transport is expected to persist in more realistic nonequilibrium strongly correlated systems.

DOI: 10.1103/PhysRevB.87.235130 PACS number(s): 05.60.Gg, 03.65.Yz, 67.85.−d

I. INTRODUCTION

Recently, the effects of noise on the efficiency of quantum transport phenomena have been scrutinized intensely by the scientific community. This has been motivated in part by a series of ground-breaking nonlinear spectroscopic experiments on light-harvesting complexes demonstrating surprisingly long-lived quantum coherence during exciton transport, even in a warm and wet environment.[1–3] Yet, for purely coherent exciton dynamics in such protein pigment networks, transport is highly suppressed due to destructive interference between different propagation pathways. Instead studies revealed that the remarkably high transport efficiency observed (above 95%) in fact emerges in combination with local noise, such as dephasing, which disrupts this interference opening up previously inhibited pathways for transmission.[4–10] Transport properties in open systems can thus not only defy the traditional understanding of when quantum effects should play a significant role, but also challenge the notion that couplings to the environment unconditionally degrade performance.

Different effects of dephasing have been studied in networks populated by single particles, in scenarios such as transport through quantum optical systems,[11] heat transport through chains of two-level systems,[12] information transmission,[13] and quantum information processing.[14] Also, interesting phenomena have been seen to emerge from the coexistence of particle-particle interactions and noise, such as glassy dynamics in ordered systems[15] and interaction impeded decoherence.[16,17] However, the interplay between noise and strong correlations induced by interactions in a many-body setting is not yet fully understood. In particular, recent numerical simulations showed that the time-of-flight expansion of a strongly interacting cold atomic gas was slow in the absence of noise and substantially increased once noise was added.[18] This raises an important question as to when and how dephasing can enhance transport in a strongly interacting system.

Here, we answer this question in the affirmative by considering a concrete example composed of spinless fermions with nearest-neighbor interactions hopping through a tight-binding chain, as depicted in Fig. 1. This model makes an ideal testbed for several reasons. First, it is equivalent to the well studied XXZ spin-1/2 chain,[19–21] representing one of the simplest models of strongly correlated electron systems. Second, the transport properties of such low-dimensional interacting quantum systems remain an important open problem, exhibiting anomalous features such as ballistic spin transport and unusually high thermal conductivity, reported experimentally in so-called spin-chain materials.[22–25] In addition to solid state systems like chains of coupled quantum dots[26] or molecular wires embedded between electrodes,[27] understanding this model is directly relevant to ion-trap,[28] coupled-cavity array,[29] and cold-atom[18,30–32] quantum systems. Of particular importance are recent seminal experiments that revealed the contact and bulk resistivity of cold fermionic atoms flowing through a narrow mesoscopic channel between a pair of reservoirs with a population imbalance.[33,34]

Very similar to these cold-atom experiments, we consider a chain attached to two unequal Markovian reservoirs at its boundaries providing continuous incoherent driving, along with local dephasing noise along its extension (see Fig. 1).[35–38] We then compute the current-driving characteristics of its nonequilibrium stationary state (NESS). Being a homogeneous chain with transport from end to end, previously studied single-particle interference effects originating from geometry or disorder are absent.[6,7,39,40] Interestingly, we show that dephasing-enhanced transport nonetheless emerges so long as the interactions are strong enough. In this regime and at maximal driving, the NESS forms a cooperative many-body quantum state possessing a long-ranged domain of particles pinned to one boundary strongly suppressing the current, analogous to a Coulomb or Pauli blockade insulator.[36] Dephasing induces incoherent transitions out of this bound

FIG. 1. (Color online) Spinless fermions hop with amplitude τ across a chain, subject to a nearest-neighbor density-density interaction of strength Δ, local dephasing at a rate γ, and boundary driving that injects/ejects fermions at a rate proportional to Γ and driving bias f. The driving process induces a forward (upper arrows) and a backward (lower arrows) flow of particles, and the bias f determines the imbalance between both.

state establishing a current in a regime that would otherwise be insulating. We illustrate this mechanism in a simple toy model, in which we isolate the essential conditions for the emergence of the effect. Surprisingly, a large current enhancement is predicted to exist in any long and finite chain even for weak driving, where the transport is diffusive in the absence of noise. We also observe that the transport enhancement is a signature of an underlying nonequilibrium phase transition, and demonstrate its generality beyond the integrable system considered.

The paper is organized as follows. In Sec. II, we describe the system to be studied. In Sec. III, we show the existence of dephasing-assisted transport for strong interactions, which contrasts with the transport degradation at weak interactions. The mechanism behind this nonequilibrium phenomenon is explained in Sec. IV. An illustrative toy model containing the basic features for the effect to emerge is described in Sec. V. The signatures of a nonequilibrium phase transition between the two transport regimes, revealed by the existence of an optimal dephasing rate and the correlations through the system, are presented in Section VI. We also show in this section that this transition remains even if the integrability of the model is broken. Finally, in Sec. VII, we discuss the conclusions of our work.

II. MODEL

We study the N site interacting spinless fermion chain described by the Hamiltonian

$$H = \sum_{j=1}^{N-1}\left[\frac{1}{2}\tau(c_j^\dagger c_{j+1} + \text{H.c.}) + \Delta\left(n_j - \frac{1}{2}\right)\left(n_{j+1} - \frac{1}{2}\right)\right], \tag{1}$$

where $c_j^\dagger, c_j$ are standard fermionic creation/annihilation operators for site j and $n_j = c_j^\dagger c_j$ is the associated number operator. In addition to the hopping amplitude τ, this Hamiltonian has a nearest-neighbor density-density interaction $n_j n_{j+1}$ with strength Δ. We take $\tau = 1$ to set the energy scale. The dynamics of the system is described by a Lindblad quantum master equation,[41] (taking $\hbar = 1$)

$$\frac{d\rho}{dt} = -i[H,\rho] + \mathcal{L}(\rho), \tag{2}$$

where ρ is the density matrix of the chain and $\mathcal{L}$ is the dissipator describing the coupling to the Markovian reservoirs. In Lindblad form, the dissipator is

$$\mathcal{L}(\rho) = \sum_k \left(L_k \rho L_k^\dagger - \frac{1}{2}\{L_k^\dagger L_k, \rho\}\right), \tag{3}$$

where $\{.,.\}$ is the anticommutator and the sum is over a set of jump operators L_k. We consider a dissipator that splits into three parts $\mathcal{L} = \mathcal{L}_L + \mathcal{L}_d + \mathcal{L}_R$. Here $\mathcal{L}_L$ and $\mathcal{L}_R$ describe the coupling to external particle reservoirs at the left and right boundaries, respectively, each with two jump operators:

$$L_{L,R}^+ = \sqrt{\Gamma(1 \mp f)/2}\, c_{1,N}, \quad L_{L,R}^- = \sqrt{\Gamma(1 \pm f)/2}\, c_{1,N}^\dagger, \tag{4}$$

where Γ is the coupling strength, identical for both reservoirs, and $0 \leqslant f \leqslant 1$ is the driving bias.[36] We consider moderate coupling $\Gamma = 1$ throughout this paper.[42] The driving mechanism, depicted in Fig. 1, induces two pumping processes, corresponding to forward (left-to-right) and backward (right-to-left) flows, thus forcing the system far from equilibrium. This scheme is reminiscent of the well studied classical stochastic exclusion model.[43,44] When $f = 0$, particles are injected and ejected with equal rates at both boundaries, so the counterpropagating flows cancel each other. This results in the stationary solution $\rho = \mathbb{1}/2^N$ to Eq. (2), irrespective of Δ, thus having no net current.[45] For $f > 0$, the forward flow is favored over the backward flow, raising the possibility of a genuine NESS possessing a finite current. The remaining contribution $\mathcal{L}_d$ accounts for bulk dephasing in the chain and is described by the jump operators

$$L_j^d = \sqrt{\gamma}(\mathbb{1} - 2n_j), \quad 1 \leqslant j \leqslant N, \tag{5}$$

with a uniform dephasing rate γ.

By directly simulating Eq. (2) and taking the long-time limit, the state $\rho(t)$ converges to the time-independent NESS of the system. A solution can be computed efficiently in a controlled way and accounting for significant many-body correlations by applying the time evolving block decimation (TEBD) algorithm[46,47] to a matrix product operator description of $\rho(t)$. This highly compact representation enables the efficient evaluation of relevant expectation values and makes accessible much larger system sizes than exact diagonalization or Monte Carlo approaches.[48–50] Moreover, TEBD can be applied effectively over a large parameter range allowing us to examine the properties of the system as a function of f beyond the $f \ll 1$ linear response regime. Our implementation of the numerical method is based on the open source tensor network theory (TNT) library.[51]

The transport properties are analyzed by computing the current crossing site j from the operator

$$J_j = i(c_j^\dagger c_{j+1} - \text{H.c.}), \quad 1 \leqslant j \leqslant N-1. \tag{6}$$

In the NESS, the current $\langle J_j \rangle = \langle J \rangle$ is homogeneous throughout the system.

III. DEPHASING ENHANCED TRANSPORT

It is known that in the weakly interacting regime $|\Delta| < 1$, in the absence of dephasing, the system is an ideal ballistic conductor for any driving f, with a nearly flat density profile $\langle n_j \rangle$ and a current $\langle J \rangle \propto f$, which is independent of N.[36,52]

The introduction of dephasing has been shown to induce diffusive transport, where the current fulfills the diffusion equation $\langle J\rangle = \kappa\nabla\langle n_j\rangle$, with κ the particle conductivity, and $\langle n_j\rangle$ features a constant gradient

$$\nabla\langle n_j\rangle = \frac{\langle n_{N-1}\rangle - \langle n_2\rangle}{N-3} = \frac{\Delta n}{N-3}, \tag{7}$$

where Δn is the density difference between opposite ends of the system (after discarding the boundary sites). As a result, the current scales with the size of the system as

$$\langle J\rangle \propto \frac{\Delta n}{N-3} \sim \frac{f}{N}, \tag{8}$$

characteristic of an Ohmic conductor.[39,53] In either case, the maximum current through the chain occurs at maximal bias $f = 1$, where only forward pumping is present, as might be intuitively expected. In the noninteracting limit, $\Delta = 0$, it has been proven rigorously that a homogeneous chain cannot exhibit any dephasing enhanced end-to-end transport;[5,40,53] this behavior was also suggested for weakly-interacting systems where $|\Delta| < 1$.[39] In Fig. 2(a), we report the current-driving profiles for $\Delta = 0.5$ showing that dephasing monotonically degrades the current for any driving, confirming that this behavior persists even in the presence of weak interactions. Thus, in this work, we focus on the strongly interacting regime $|\Delta| > 1$.

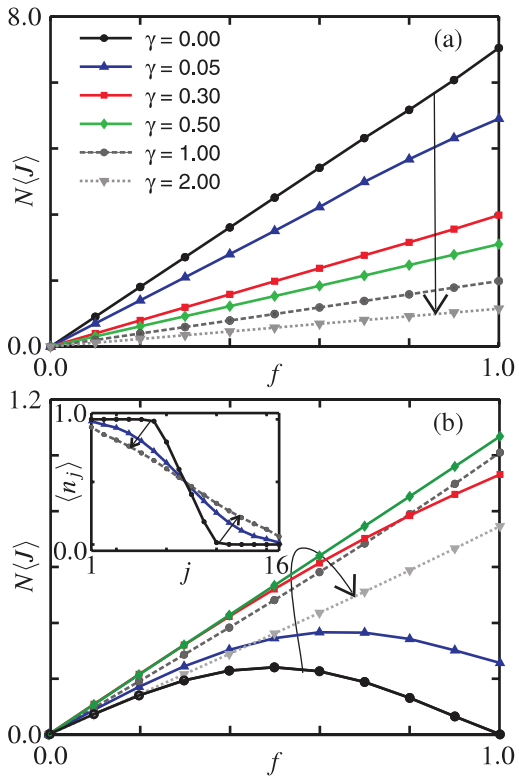

FIG. 2. (Color online) (a) The current-driving profiles in the weakly interacting regime $\Delta = 0.5$ for increasing (as indicated by the arrow) dephasing rates γ and $N = 16$. (b) Identical plot to (a) but in the strongly interacting regime $\Delta = 2$. (Inset) The density $\langle n_j\rangle$ of the system when $\Delta = 2$, $f = 1$, and $N = 16$, corresponding to $\gamma = 0, 0.05, 1.00$.

In the absence of dephasing and for weak driving $f \ll 1$, transport was found to be diffusive when $|\Delta| > 1$,[52] a controversial finding given that the integrability of the system is conjectured to lead to ballistic transport.[54] However, for strong driving, $f \to 1$, it was recently discovered[36,55] that the NESS exhibits a particle domain at the left edge of the chain irrespective of the sign of Δ, strongly suppressing the current as $\langle J\rangle \propto \exp(-N)$, characteristic of an insulator. Consequently, the current $\langle J\rangle$ at $\gamma = 0$ exhibits nonlinear behavior with the driving f, leading to an effect known as negative differential conductivity (NDC) where increasing the driving eventually decreases the current.[36,55] In Fig. 2(b), the $\gamma = 0$ curve shows that this causes a near complete suppression of the current at $f = 1$ for $\Delta = 2$. In the strongly interacting regime, the system therefore presents the intriguing property that more current forward flows at an intermediate bias $f < 1$ where some backward pumping is present.

A. Current enhancement

The main result of the present work is that for $|\Delta| > 1$ the presence of a small bulk dephasing can significantly enhance the particle transport. This striking behavior is illustrated for $\Delta = 2$ in Fig. 2(b) where dephasing up to a moderate rate $\gamma \approx 0.5$ is seen to increase the current. This enhancement in the current is shown to occur *for any* $f > 0$; however, it is not uniform in f, resulting in the current-driving profile changing with γ. Specifically, around $\gamma \approx 0.3$ the NDC effect is lost and further increases in γ yield a linear profile in f. Near $f = 1$, dephasing therefore induces not just a quantitative increase in the current, but rather causes a major qualitative change in the behavior of the system from being insulating at $\gamma = 0$ to yielding the maximal current once $\gamma > 0.3$. In the inset of Fig. 2(b), this change at $f = 1$ is shown to be coincident with the breakdown of the particle domain at the left boundary into a nearly linear density profile, due to the increase of the dephasing rate. The transport at large driving and dephasing rates therefore resembles that of a diffusive conductor. This result is confirmed by the scaling of the current with the size of the system, shown in Fig. 3 for $\Delta = 2$ and dephasing rates $\gamma = 0.5$ and $\gamma = 1.0$. The power-law fits for each γ, which are seen to accurately model the data, indicate subdiffusive transport for $\gamma = 0.5$, where the current decays slower than $1/(N-3)$, but has approached a diffusive behavior once $\gamma = 1.0$.

For a given f there is an optimal dephasing rate $\gamma_{\rm opt}$ that maximizes the current, as shown in Fig. 4. For the parameters of this figure, the enhancement at weak driving and the optimal dephasing rate is quite significant, e.g., $\approx$37% at $f = 0.1$. As the driving increases so does the optimal dephasing rate $\gamma_{\rm opt}$, as well as the enhancement of the current, the latter being of several orders of magnitude for $f \to 1$. For $\gamma > \gamma_{\rm opt}$, the current is reduced because the $\mathcal{L}_d$ contribution to Eq. (2) dominates over the coherent hopping terms and progressively freezes out the dynamics due to the Zeno effect.[41] In fact, for increasingly large γ, the NESS current converges to the exact $\Delta = 0$ solution with dephasing:[53,56]

$$\langle J\rangle_{\Delta=0} = \frac{2f}{\frac{\Gamma}{4} + \frac{4}{\Gamma} + (N-1)\gamma}. \tag{9}$$

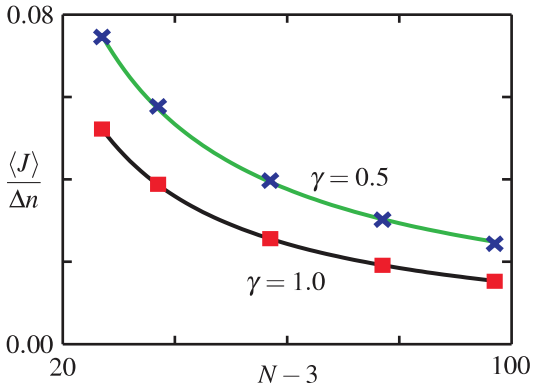

FIG. 3. (Color online) The current $\langle J\rangle$ at $f = 1$, divided by the resulting density difference Δn between the ends of the system (excluding the boundary), is plotted against the system size $N-3$ up to $N = 100$ sites. The data is for dephasing rates $\gamma = 0.5$ (×) and $\gamma = 1.0$ (■). The solid lines show the fitting to $\langle J\rangle/\Delta n = \kappa(N-3)^{-\alpha}$ for each γ. These yield $\kappa = 1.288$ and $\alpha = 0.863$ for $\gamma = 0.5$, and $\kappa = 1.228$ and $\alpha = 0.958$ for $\gamma = 1.0$.

This convergence, shown in Fig. 4, thus indicates that the interaction strength Δ becomes irrelevant for very large dephasing rates.

B. Scaling with the system size

To show that the transport enhancement is not restricted to small chains, we analyze the scaling of the optimal dephasing rate $\gamma_{\rm opt}$ with N for weak driving $f = 0.1$. The results are presented in Fig. 5. Although $\gamma_{\rm opt}$ decreases as N increases, extrapolations with simple trial functions (of which an exponential decay, shown in Fig. 5, gives the best description) indicate that even when $N \to \infty$, $\gamma_{\rm opt}$ remains finite. However, since the density imbalance between the boundaries of the chain Δn is bounded, $\langle J\rangle \to 0$ in the thermodynamic limit; see also the inset of Fig. 5, which shows that $\langle J\rangle_{\rm opt} \to 0$ as $N \to \infty$. Nevertheless, the existence of a finite $\gamma_{\rm opt}$ in the thermodynamic limit indicates that even in the linear response regime, the transport can be enhanced

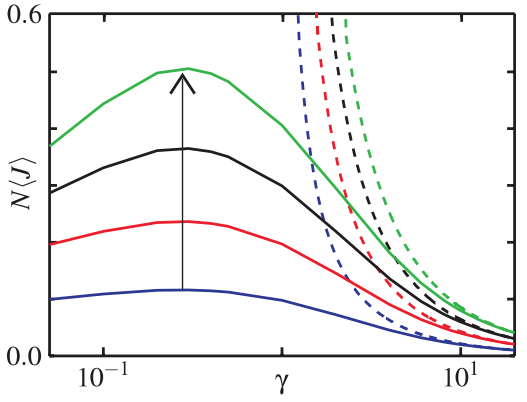

FIG. 4. (Color online) The current as a function of γ for driving biases $f = 0.1$, 0.2, 0.3, and 0.4 (from bottom to top curve) with $\Delta = 2$, and $N = 40$. The dashed lines correspond to $\langle J\rangle_{\Delta=0}$, the noninteracting analytic result.[53,56]

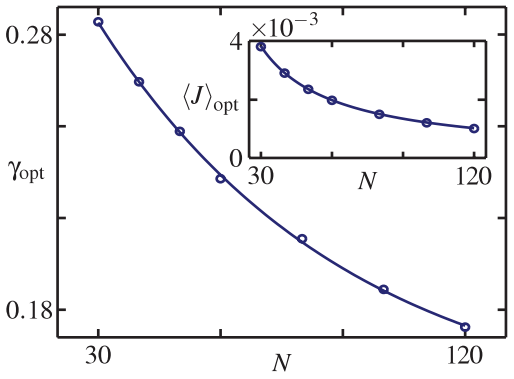

FIG. 5. (Color online) Optimal dephasing $\gamma_{\rm opt}$ for different sizes of the system, at $f = 0.1$, $\Delta = 2$, and $\Gamma = 1$ (circles). The solid line corresponds to the exponential decay $\gamma_{\rm opt} = \gamma_{\rm opt}^{\rm TL} + a\exp(-N/b)$, with $a = 0.252$, $b = 85.9$, and $\gamma_{\rm opt}^{\rm TL} = 0.109$. (Inset) Optimal current $\langle J\rangle_{\rm opt}$ as a function of N. The solid line corresponds to the power law decay $\langle J\rangle_{\rm opt} = aN^{-b}$, with $a = 0.0948$ and $b = 0.94$. Note that as $N \to \infty$, $\langle J\rangle_{\rm opt} \to 0$.

by environmental coupling in systems of *any* finite size. For stronger driving, both the current enhancement and $\gamma_{\rm opt}$ become larger, as shown in Fig. 4, and the range of beneficial dephasing rates broadens. So the dephasing-enhanced transport should emerge in mesoscopic systems even for weak driving.

IV. ENHANCEMENT MECHANISM

We now discuss the physical mechanism underlying NDC and the dephasing enhanced transport. Specifically, we show that these effects arise due to an interplay between the eigenstructure of the strongly interacting chain Hamiltonian and the boundary driving. As illustrated in Fig. 6(a) for a small but representative system size with very strong interactions $|\Delta| \gg 1$, the eigenspectrum consists of nearly flat high-energy bands of bound states of low conductivity, separated by gaps of order $|\Delta|$ from more mobile bands of states with lower energy. As we shall now show, strong boundary driving preferentially populates only the most energetic bound states resulting in an insulating NESS. The introduction of dephasing then induces transitions to mobile current-carrying bands, thereby enhancing the conductivity.

To see this in more detail, it is instructive to first consider maximally biased driving $f = 1$ in the extreme $|\Delta| \to \infty$ limit. In this case, configuration states such as $|10110\cdots011\rangle$, where the particle occupancy on each site of the chain is explicitly specified, are exact eigenstates of the Hamiltonian. A key property of the boundary driving is that it only incoherently connects configurations within a quadruplet of states $|0\mathbf{x}0\rangle, |0\mathbf{x}1\rangle, |1\mathbf{x}0\rangle, |1\mathbf{x}1\rangle$ for any value of f, where $\mathbf{x}$ is any length $N-2$ occupancy bit string and thus defines each quadruplet. This is illustrated in Fig. 6(b). Consequently, if $\mathbf{x}$ has $(n-1)$ 1's, the driving couples states within the total particle number sectors $n-1, n$, and $n+1$. This structure constrains the evolution caused by the driving processes to shuffling population between states in these isolated quadruplets. At $f = 1$, there is one configuration $|1\mathbf{x}0\rangle$ within each quadruplet which, owing to it having a

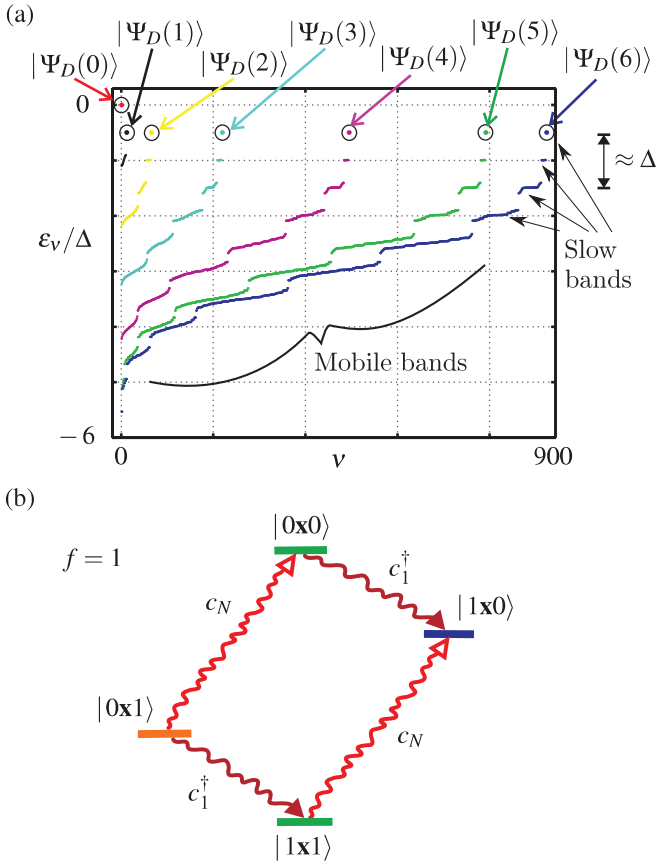

FIG. 6. (Color online) (a) The energy eigenspectrum of the spinless fermion Hamiltonian governing the chain for $N = 12$ and $\Delta = 10$. Energies ϵ_ν have been shifted by $\frac{1}{4}\Delta(N-1)$ so that the state $|\Psi_D(0)\rangle = |00\ldots00\rangle$ has zero energy. The spectrum includes contributions from all particle number sectors $n = 0, \ldots, 12$; since the spectra arising from $n = 0, \ldots, 5$ are identical to those of $n = 7, \ldots, 12$, only the former are shown in addition to $n = 6$. The highest lying eigenstate for each sector $|\Psi_D(n)\rangle$ is highlighted and seen to be isolated by a gap of $O(\Delta)$ from eigenstates composed of break-away configurations (states with the outermost particle of the domain breaking away, or a hole propagating through the domain). The braces give an indication of the location of mobile and flattened bands for $n = 6$. (b) For any f, the driving alone incoherently connects a quadruplet of configurations $|0\mathbf{x}0\rangle, |0\mathbf{x}1\rangle, |1\mathbf{x}0\rangle, |1\mathbf{x}1\rangle$. The situation for $f = 1$ is shown where the driving can be seen to only pump into the so-called dark configuration $|1\mathbf{x}0\rangle$.

particle on the leftmost site and a vacancy on the rightmost site, is entirely decoupled from the driving (i.e., there is no action of the driving on such a configuration), while also being the sink for all driving transitions [see Fig. 6(b)]. The effect of this incoherent evolution alone is thus to eventually drive all the population among the quadruplet of states into this *dark configuration*. Of particular relevance are the dark configurations

$$|B_n\rangle = |\overbrace{111\cdots111}^{n}\underbrace{000\cdots000}_{N-n}\rangle, \tag{10}$$

which possess an n particle domain pinned to the left boundary. For each particle number sector n, the state $|B_n\rangle$ is separated from other configurations by an energy gap $O(|\Delta|)$, akin to a domain binding energy.

As we move to the limit of finite, but strong interactions $|\Delta| \gg 1$, hopping between configuration states results in each configuration $|B_n\rangle$ giving rise to an eigenstate $|\Psi_D(n)\rangle$ of bound particles. For each particle number n, $|\Psi_D(n)\rangle$ is the highest state in the eigenspectrum, as indicated in Fig. 6(a). Its properties are readily determined by treating hopping as a perturbation. Specifically, to lowest-order in $|2\Delta|^{-1}$, hopping hybridizes, across an energy gap of Δ, the state $|B_n\rangle$ with the break-away configuration

$$|\overbrace{111\cdots11}^{n-1}01\underbrace{00\cdots000}_{N-n-1}\rangle, \tag{11}$$

where the outermost particle of the domain has escaped. As discussed in Appendix A, the hybridization of $|B_n\rangle$ with more distant break-away configurations decays exponentially with the distance from the domain wall with a length scale $\xi \sim 1/\ln(|2\Delta|)$. Crucially almost all of these break-away configurations are dark to the driving like $|B_n\rangle$. Only the configurations where either a hole or particle has reached the boundary couple to the driving, and their amplitude is exponentially suppressed by this localization.

The emergence of an insulating NESS in the strongly interacting regime at $f = 1$, having a particle domain of size $N/2$, and thus the domain wall farthest from the boundaries, follows from the combination of two results in the perturbative approach: (i) as $n \to N/2$, $|\Psi_D(n)\rangle$ becomes an exponentially close approximation to a dark state of $f = 1$ driving, with increasing N. (ii) The boundary driving at $f = 1$ preferentially populates $|\Psi_D(n)\rangle$ leaving a NESS that is well approximated by a statistical mixture

$$\rho = \sum_{n=0}^{N} p_n |\Psi_D(n)\rangle\langle\Psi_D(n)|, \tag{12}$$

with the probability p_n exponentially peaked at $n = N/2$. In Appendix A, points (i) and (ii) are shown to arise for sizes $N \geqslant 4$.

The existence of the insulating NESS described by Eq. (12) is only possible in the absence of dephasing processes along the chain. Since local dephasing on each site, given in Eq. (5), does not commute with the chain Hamiltonian H, this noise process induces incoherent transitions between many-body energy eigenstates of the system. This is characterized by an energy dissipation rate

$$\frac{dE_\gamma}{dt} = -2\gamma \sum_j \langle c_j^\dagger c_{j+1} + \text{H.c.}\rangle, \tag{13}$$

dependent on the kinetic energy of the state, and enables population to escape from the approximate dark states $|\Psi_D(n)\rangle$ to the mobile bands of scattering states. It is this effect that breaks the localization in the $f = 1$ insulating NESS and significantly enhances the current. An optimal dephasing rate γ_{opt} emerges due to the competition between these dephasing induced transitions and the degradation of mobility of the scattering states by dephasing through the Zeno effect. An increase in γ_{opt} with $|\Delta|$ is observed

since a larger energy dissipation is needed to overcome the gap.

When reducing f slightly from the $f = 1$ limit, a small backward pumping process appears in addition to the dominant forward pumping of particles. Since particles are then injected and ejected by the driving at both boundaries, all the states of every quadruplet become populated and there are no longer dark configurations decoupled from the driving. A finite current is therefore established in the NESS as the population in the approximate dark states $|\Psi_D(n)\rangle$ diminishes. Nonetheless, the picture of dissipation from majority occupied bound states to higher mobility scattering states still applies. However, in the linear response regime, where $f \to 0$ and the NESS is a diffusive conductor rather than an insulator, it is not *a priori* obvious that additional dissipation induced by dephasing will be beneficial to transport. Yet, as seen in Figs. 4 and 5, an enhancement of the current due to dephasing for chains of any finite size is observed for $f > 0$. This behavior suggests that even in this case, where the high-energy bound states like $|\Psi_D(n)\rangle$ are only marginally populated by the driving, additional incoherent transitions bridging the numerous gaps in the spectrum to the mobile bands still enhance transport. To help further unravel the processes behind dephasing enhancement and NDC, we describe a simple toy model in the following section. This model not only reproduces the basic features of these effects in a concrete analytically tractable way, but also reveals that the physical mechanism underlying both effects is the same.

V. TOY MODEL

We have seen that numerous approximate dark states, whose occupation is favored by $f = 1$ driving, cause the stationary state to become insulating. Remaining in the strongly interacting limit, we now wish to isolate the effect of such bound states on the transport for all drivings f, i.e., on the complete current-driving profile. To do so, we construct a simple toy model, whose structure is motivated by considering the half-filled domain state $|B_{N/2}\rangle$ and its corresponding break-away configurations, which eventually connect it to the boundary driving. As such, the toy model is composed of K configuration states $|1\rangle,|2\rangle,\ldots,|K\rangle$ for some size $K > 2$. To mimic the interaction binding energy of $|B_{N/2}\rangle$, we distinguish the configuration $|K\rangle$ by elevating it in energy by Δ above the set of otherwise degenerate configurations $|1\rangle,|2\rangle,\ldots,|K-1\rangle$, which model break-away states like $|11\cdots10100\cdots0\rangle$, $|11\cdots10010\cdots0\rangle$, etc. In addition, the states $|1\rangle,|2\rangle,\ldots,|K\rangle$ are also coherently coupled to their neighbors via "hopping" processes given by

$$H_t = \frac{1}{2}\sum_{k=1}^{K-1}(|k\rangle\langle k+1| + \text{H.c.}).$$

The current operator for the model then follows as

$$J = -i\sum_{k=1}^{K-1}(|k\rangle\langle k+1| - \text{H.c.}),$$

which measures the flow within the coherently connected configurations $|1\rangle,|2\rangle,\ldots,|K\rangle$. To model the driving in the full system, which incoherently connects one particle number sector to another, we introduce an auxiliary state $|s\rangle$ whose function is simply to be an intermediary. The jump operators describing the driving then take the form

$$L_L^{\pm} = \sqrt{\Gamma(1\mp f)/2}\,\Lambda_L^{\pm}, \quad L_R^{\pm} = \sqrt{\Gamma(1\pm f)/2}\,\Lambda_R^{\pm},$$

where $\Lambda_L^- = |s\rangle\langle 1|$ and $\Lambda_R^+ = |K\rangle\langle s|$, with $\Lambda_L^+ = (\Lambda_L^-)^\dagger$ and $\Lambda_R^- = (\Lambda_R^+)^\dagger$. Thus, via $|s\rangle$, the driving incoherently induces transitions between the boundary configurations $|1\rangle$ and $|K\rangle$ with a bias f. At $f = 0$, driving in both directions is equal and it is easily confirmed that the NESS is $\rho = \mathbb{1}/(K+1)$, yielding $\langle J\rangle = 0$ as in the case of the full spinless fermion chain. At the opposite limit, $f = 1$, population is asymmetrically driven from $|1\rangle \to |K\rangle$. To complete the analogy with the full system, the toy model also includes dephasing, at a rate γ, via the jump operator $L_Z = \sqrt{\gamma}\Lambda_Z$ where

$$\Lambda_Z = \mathbb{1} - 2\,|K\rangle\langle K|,$$

whose action is to scramble the phase of any superpositions between $|K\rangle$ and the other configurations. A schematic of the toy model illustrating all the coherent and incoherent contributions is shown in Fig. 7.

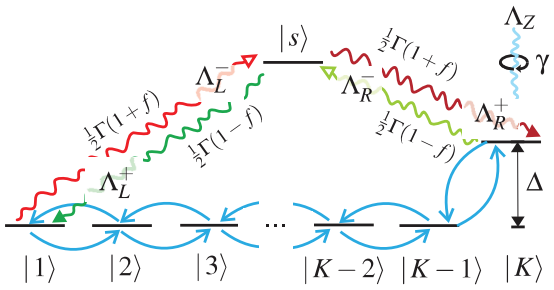

FIG. 7. (Color online) The schematic of the toy model and its various processes and properties. These include the nearest-neighbor coherent hopping between the set of states $|1\rangle,|2\rangle,\ldots,|K\rangle$, an energy offset Δ for state $|K\rangle$, incoherent transitions $|1\rangle \leftrightarrow |s\rangle$ and $|K\rangle \leftrightarrow |s\rangle$ between the boundary states and the auxiliary state $|s\rangle$, and dephasing at a rate γ. The rates for the incoherent driving transitions $\frac{1}{2}\Gamma(1 \pm f)$ are also listed.

Since it is inspired in the $|\Delta| \gg 1$ regime, the toy model does not embody the entire physics of the full system. Nevertheless, it does capture the essential features of NDC and dephasing enhancement when $|\Delta| \gg 1$. Fundamentally, the same mechanisms observed in such a limit apply to the more complex full system when considering its entire eigenspectrum, even when $|\Delta| \to 1$.

The current $\langle J\rangle = \text{tr}(J\rho)$ of the NESS ρ can be solved analytically for the toy model as a function of f, γ, and Δ, although the complete expression is lengthy. Since the model was motivated by the perturbative limit $|\Delta| \gg 1$, the physically relevant part of this result is found by keeping only the lowest order terms in Δ^{-1}. This gives

$$\langle J\rangle \approx \frac{(K-1)[8\gamma f + (1-f)f\Gamma]}{(K+1) - 2(K-2)f + (K-1)f^2}\left(\frac{1}{\Delta}\right)^2. \quad (14)$$

In Fig. 8(a), the current-driving profile $\langle J\rangle$, rescaled by Δ^2, is plotted for $K = 20$. Two key features emerge from this result. First, for $\gamma = 0$, the $(1-f)f$ in the numerator of Eq. (14), which enforces zero current at the $f = 0$ and 1, causes $\langle J\rangle$ to

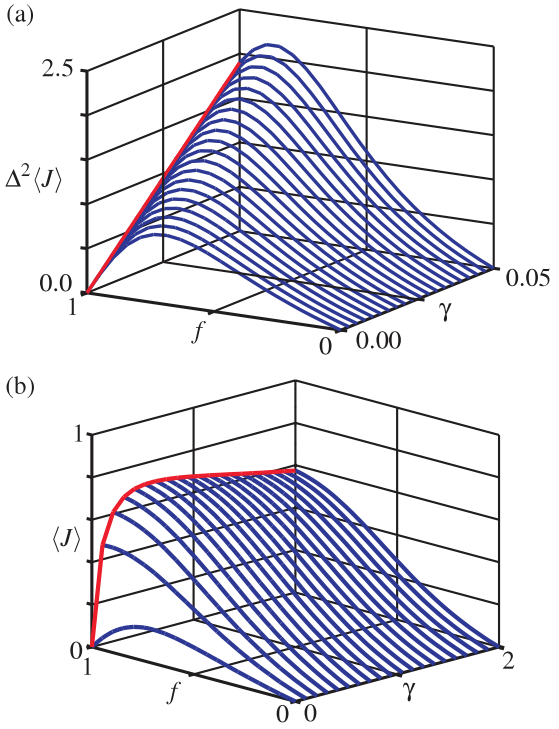

FIG. 8. (Color online) (a) The NESS current $\langle J\rangle$, rescaled by Δ^2, for $K = 20$, as a function of the driving f and dephasing γ, described by the approximation in Eq. (14). The behavior at $f = 1$ with γ is emphasized by the additional (red) line. (b) The exact current-driving profiles of the toy-model as a function of γ with $\Delta = 2$ and $K = 20$.

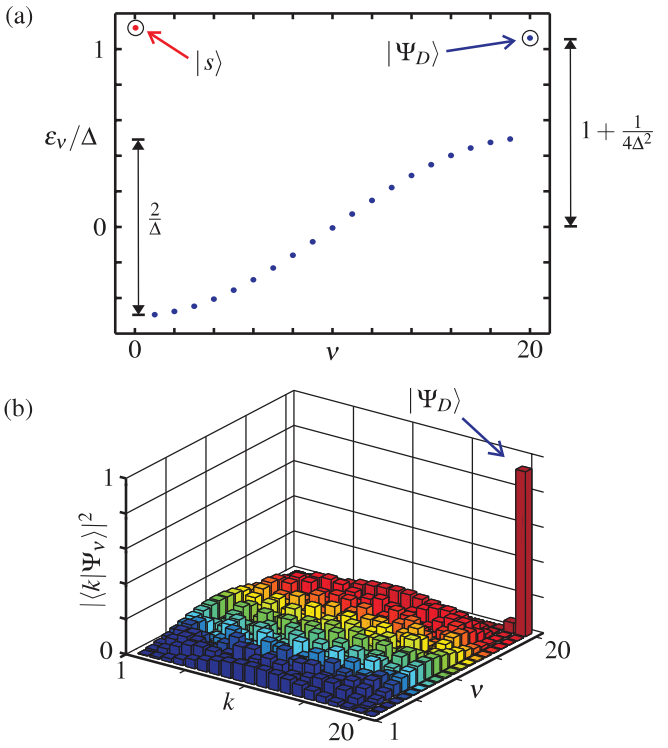

FIG. 9. (Color online) (a) The spectrum ϵ_ν of the Hamiltonian for the toy model for $K = 20$ and $\Delta = 2$. Eigenstate $\nu = 0$ is the highlighted auxiliary state $|s\rangle$ whose energy has been set arbitrarily. The highest-lying eigenstate $\nu = K$ is also highlighted and is the approximate dark state of the model $|\Psi_D\rangle$. Beneath this state, separated by a gap $O(|\Delta|)$, is a band of eigenstates $|\Psi_\nu\rangle$ split by the small hopping. (b) The probability distributions $|\langle k|\Psi_\nu\rangle|^2$ of the eigenstates over the configurations $|k\rangle$ are shown. The band of eigenstates is seen to be delocalized over the configurations $|1\rangle, |2\rangle, \ldots, |K-1\rangle$ and expunged from the boundary configuration $|K\rangle$, while the characteristic of a bound state $|\Psi_D\rangle$ is predominately peaked at $|K\rangle$ with exponential tail into the bulk.

display negative differential conductivity (NDC). Moreover, the expansion involves only even powers of Δ^{-1}, showing that this behavior is independent on the sign of Δ. Second, dephasing enhancement of $\langle J\rangle$ is evident from the linear γ term in Eq. (14), which eventually destroys the NDC effect. However, since γ and Γ appear only linearly, this lowest order expression is only valid for weak dephasing and coupling to the boundary reservoirs. In particular, the dephasing degrading behavior expected for large γ, due to the Zeno effect, is not described by Eq. (14). The expression is also only valid for $K \geqslant 3$ because NDC is not seen for $K = 2$; having no direct coherent coupling between the boundary configurations where driving occurs, i.e., $|1\rangle$ and $|3\rangle$ for $K = 3$, is essential for NDC to emerge. This is similar to how NDC is only seen for $N \geqslant 4$ in the full system, like in Fig. 14(b) of Appendix A. In Fig. 8(b), the exact current-driving profile for the toy model is shown for $\Delta = 2$ as a function of moderate γ's, beyond the applicability of Eq. (14). This confirms the wider similarity of the response of the toy model to that observed in the full spinless-fermion system.

Given their similar response, the toy model provides a tractable means of unravelling the origins of NDC and dephasing enhancement in the full many-body system. The eigenspectrum of the toy model is plotted in Fig. 9(a). By construction, we see that it mimics some of the features shown in Fig. 6(a) for an individual number sector of the spinless fermion system. Specifically, there is a high-lying eigenstate $|\Psi_D\rangle$, separated by a gap $O(|\Delta|)$ from a dense band of eigenstates. In Fig. 9(b), the eigenstates of this band are seen to be delocalized over the bulk of the system excluding the boundary configuration $|K\rangle$. In contrast, for a given size K, the eigenstate $|\Psi_D\rangle$ has the form

$$|\Psi_D\rangle \approx \sum_{k=0}^{K-1} |2\Delta|^{-k} |K-k\rangle, \tag{15}$$

to within $O(|2\Delta|^{-2K})$. So as seen in Fig. 9(b), $|\Psi_D\rangle$ is exponentially peaked at $|K\rangle$. As $K \to \infty$, such an exponentially decaying wave function is simply the discrete analog of the well-known bound state of a 1D δ potential.[57] Given that the amplitude for the left boundary configuration $|1\rangle$ scales as $|2\Delta|^{1-K}$, we see that $|\Psi_D\rangle$ becomes exponentially close, with increasing K, to being a dark state of the driving when $f = 1$.

The driving at $f = 1$ exclusively pumps into the configuration $|K\rangle$ whose dominant overlap is with $|\Psi_D\rangle$. Consequently, so long as $\gamma = 0$, the population gets progressively trapped in this dark state giving rise to $\langle J\rangle \approx 0$, characteristic of an insulating NESS. Remaining at $f = 1$ and switching on a nonzero dephasing directly decoheres the exponentially

decaying superposition within $|\Psi_D\rangle$. This is equivalent to the coherent trapping of population, caused by the energetic gap, being bypassed by dephasing induced incoherent transitions connecting $|\Psi_D\rangle$ directly to the delocalized band of eigenstates. Current flow in the system is thus made possible via the ensuing nonstationary mixture of these eigenstates. Further increases in dephasing eventually degrade the current once the monotonically decreasing mobility of the delocalized eigenstates, caused by the Zeno effect, outweighs the flux of population escaping from $|\Psi_D\rangle$. Since the toy model only has a single approximate dark state $|\Psi_D\rangle$, it confirms that its existence, at one isolated point $f = 1$ and $\gamma = 0$, is alone enough to make the current-driving profile for $0 \leqslant f \leqslant 1$ exhibit NDC and $\gamma > 0$ exhibit dephasing enhancement.

Another key insight from the toy model is that the emergence of a nonzero current from the insulating point $f = 1$ and $\gamma = 0$, involves identical physics either when γ is increased slightly from zero, or when f is reduced slightly from unity. Examining Eq. (14) at $f = 1$ shows that $\langle J\rangle\Delta^2 = 2(K-1)\gamma$, while for $\gamma = 0$ an expansion about $f = 1$ shows that the current is $\langle J\rangle\Delta^2 = \frac{1}{4}(K-1)(1-f)\Gamma$ to lowest order. This suggests a correspondence

$$\gamma = \frac{1}{2}(1-f)\frac{\Gamma}{4}. \tag{16}$$

Consequently, a slight decrease of driving or increase of dephasing induce the same decoherence process that enhances the transport of the otherwise insulating state. A further indication of this equivalence, focused on the decay in time of the coherences between states $|K-1\rangle$ and $|K\rangle$, is presented in Appendix B.

While successful in describing the effective single-particle aspects of the full spinless fermion system, the toy model fails to describe several important features that are hallmark of genuine many-body physics. First, in the strongly driven $f = 1$ limit at large dephasing, the toy model does not display diffusive transport, like that observed for the full system in Fig. 3. This is expected since aside from configuration $|K\rangle$ the toy model is an ordered homogeneous tight-binding system. Second, when there is no dephasing, the full system is known to exhibit a nonequilibrium phase transition from diffusive to ballistic transport at weak driving[36] as $|\Delta| \to 1$. As the toy model was constructed to mimic the $|\Delta| \gg 1$ limit, it does not capture this many-body property of the full system. In the next section, we investigate the effect of dephasing on this transition in the full system.

VI. SIGNATURE OF A NONEQUILIBRIUM PHASE TRANSITION

The results discussed in Sec. III demonstrate the existence of two transport regimes in the system with different responses to moderate dephasing: degradation for weak interactions and enhancement for strong interactions. We now discuss the transition between the two transport regimes, characterize the critical interaction strength, analyze the correlations through the system for each regime, and show that the same regimes of response remain even when the integrability of the system is broken.

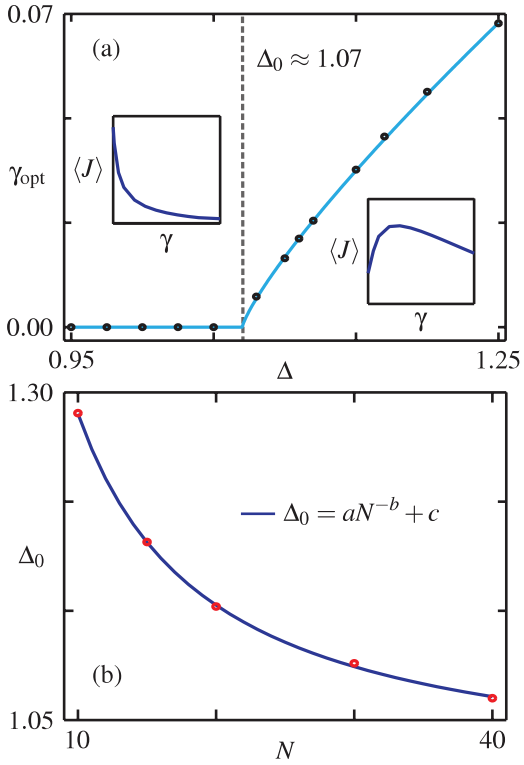

FIG. 10. (Color online) (a) The optimal dephasing rate $\gamma_{\rm opt}$ as a function of Δ, for $N = 40$, $f = 0.1$, and $\Gamma = 1$. The circles indicate TEBD results, and the solid line corresponds to the fitted function $\gamma_{\rm opt} \propto (\Delta - \Delta_0)^\beta$, with $\beta = 0.819$ and $\Delta_0 = 1.07$. The inset plots show the generic behavior of $\langle J\rangle$ with γ above and below Δ_0. (b) The scaling of Δ_0 with N for $f = 0.1$ and $\Gamma = 1$, along with the fitted power-law shown, where $a = 3.906$, $b = 1.066$, and $c = 0.995$.

A. Transition at $|\Delta| = 1$

The interaction strength $|\Delta| = 1$ is of particular significance to the Hamiltonian of Eq. (1). At zero-temperature and in the absence of magnetic field, it separates the gapless and magnetically ordered (ferro- and antiferromagnetic) gapped equilibrium phases. More generally, it divides a continuous eigenspectrum for $|\Delta| < 1$ from one with numerous gaps for $|\Delta| > 1$,[58,59] as illustrated in Fig. 6(a). In the system driven by the jump operators of Eq. (4), it was previously observed that $|\Delta| \approx 1$ also separates ballistic and diffusive transport regimes for weak driving.[36] However, it is not *a priori* clear that $|\Delta| = 1$ necessarily separates the regimes of transport degradation and enhancement by dephasing. We now show that this is indeed the case.

In Fig. 10(a), the optimal dephasing rate $\gamma_{\rm opt}$ is shown for weak driving as a function of Δ. A threshold of $\Delta_0 \approx 1.07$ is apparent where for $|\Delta| < \Delta_0$, $\gamma_{\rm opt} = 0$, indicating dephasing-degraded transport, while for $|\Delta| > \Delta_0$, $\gamma_{\rm opt}$ is nonzero, indicating dephasing-enhanced transport, and increases monotonically with $|\Delta|$. The latter behavior is a consequence of the enhancement mechanism. As the interaction strength increases, so do the gaps between flattened and mobile bands, so a larger energy dissipation is required to populate the latter and increase the current. The value of Δ_0 is size-dependent, and a scaling analysis shown in Fig. 10(b) demonstrates that,

to good approximation, $\Delta_0 = 1$ separates the two transport regimes in the thermodynamic limit.

From the results discussed above, it is tempting to associate the nature of the ground state, namely gapped or gapless, with a certain type of particle transport or response to dephasing. This impression is misleading, as can be understood by considering a homogeneous on-site potential $B\sum_j n_j$. This potential shifts the equilibrium quantum critical points,[59] but leaves the particle transport of the steady state unaltered. The latter occurs because the Hamiltonian and the current operator are particle-conserving, so the sectors of different particle numbers are only incoherently connected due to the driving and the NESS is block diagonal. The internal structure of the various particle number sectors, unmodified by the homogeneous on-site potential, is thus what determines the steady-state transport through the chain, not the relative positions of the different sectors within the eigenspectrum.[60] This shows that a qualitative change of the ground state does not imply a change of nonequilibrium properties. Instead, it is the overall structure of the eigenspectrum that leads to the NDC and dephasing-enhanced transport effects at strong interactions, as discussed in Secs. IV and V.

B. Correlations and dephasing

Similar to equilibrium phases, the transition between the two different transport regimes, namely of current degradation and enhancement by dephasing, can also be distinguished from the correlations through the system. First, we consider a typical two-point density-density correlation function

$$C_{ij} = \langle n_i n_j \rangle - \langle n_i \rangle \langle n_j \rangle, \tag{17}$$

with sites i and j symmetrically positioned around the center of the chain. This is conveniently represented as $C(r)$ where $r = |i - j|/N$ is the fractional separation of the points for the system size N. In Fig. 11(a), $C(r)$ is plotted for different sizes N in the strongly interacting regime for a moderate dephasing rate. Finite correlations are seen to exist even for a large fractional separation r. Although these correlations decay with r, the fraction of the system they span increases with N. This property has been argued, for $\gamma = 0$ and $|\Delta| > 0.91$, to be evidence that the NESS possesses genuine long-range order even in the thermodynamic limit.[62] Here, our results indicate that this long-range order persists even in the presence of moderate dephasing, and so correlations similar to those at $\gamma = 0$ exist in the dephasing enhanced NESS. The situation for strong dephasing, shown in Fig. 11(b), is markedly different. Now correlations are smaller and diminish faster with r than at weaker dephasing rates. In addition, the fraction of the system over which the correlations extend diminishes as N increases, a behavior previously observed for weak interactions and $\gamma > 0$, as well as for large dephasing rates γ independently of the interaction strength $|\Delta|$.[39,53] So like the current and density profiles, the two-point correlation functions in the strongly interacting regime become increasingly similar to those of the weakly interacting regime for large dephasing, washing out the transition.

The signature of the nonequilibrium transition between weakly and strongly interacting regimes with moderate dephasing, already suggested by two-point correlation functions, can be refined by adopting a more general measure of correlations. Specifically, we compute the entropy[46,52,61]

$$S = -\sum_\alpha \lambda_\alpha^2 \log_2 \lambda_\alpha^2 \tag{18}$$

of the Schmidt coefficients λ_α arising when the full NESS density operator ρ is factorized into two half-chains as

$$\rho = \sum_\alpha \lambda_\alpha O_\alpha^A O_\alpha^B, \tag{19}$$

where O_α^A and O_α^B are Hilbert-Schmidt orthogonal operators for the two halves. Both quantum and classical correlations between the two halves of the chain are quantified by S, which is readily accessible from the TEBD numerics. For zero dephasing and weak driving, Fig. 12 shows that S peaks at $\Delta \approx 1$. This indicates that a significant elevation in correlations occurs as the NESS reorganizes itself across the expected nonequilibrium phase transition between ballistic and diffusive transport in this region.

In Fig. 12, we also show that for finite dephasing the entropy S monotonically decreases with γ, but interestingly the peak is maintained for moderate rates, shifting slightly to larger Δ. Therefore the abrupt on-set of dephasing enhancement shown in Fig. 10 occurs when the many-body correlations are strongest, indicating that it is an effect that applies far

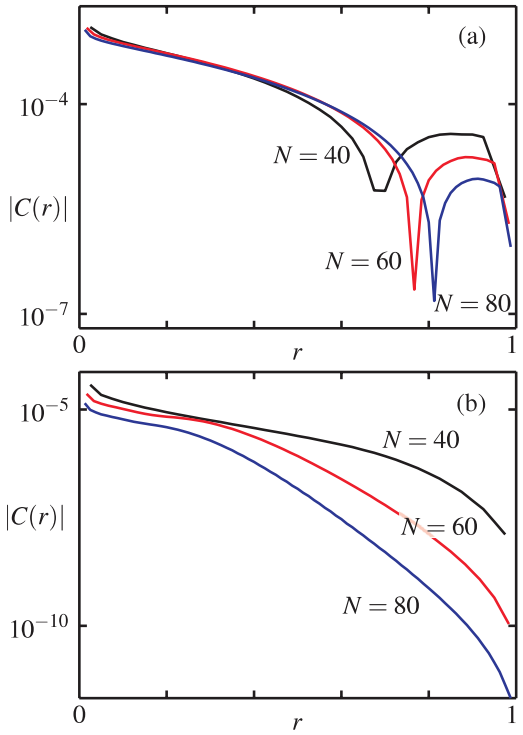

FIG. 11. (Color online) The NESS density-density correlations $|C(r)|$ across the chain as a function of the fraction distance r about the center for $\Delta = 2$ and $f = 0.1$. In (a), a moderate dephasing $\gamma = 0.05$ is included. The correlations are long-ranged and extend over a larger fraction when increasing N. This is evidenced by the kink, coming from $C(r)$ changing sign, moving to larger r. In (b), a strong dephasing $\gamma = 1$ is present and the correlations are short ranged, as shown by their diminishing size and extent with increasing N.

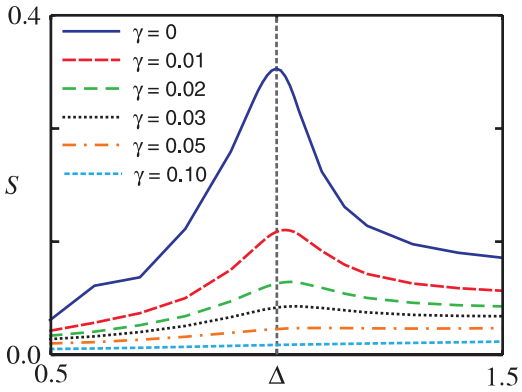

FIG. 12. (Color online) The half-chain entropy S as a function of Δ for different γ's, $f = 0.1$, and $N = 40$. The Schmidt coefficients λ_α were normalized so the largest coefficient is $\lambda_1 = 1$.

beyond the effective single-particle picture of the toy model. This distinguishing feature in S is progressively washed out by increasing the dephasing as the system becomes diffusive for all Δ.[39,53,56] Despite this, the response of the system to the dephasing processes is seen to offer an alternative and clear signature of the underlying nonequilibrium phase transition between two qualitatively different steady states.

C. Enhancement and integrability

The Hamiltonian in Eq. (1) describing the full system is integrable,[58] so it could be considered that the dephasing enhancement observed in the present work is an artifact of this property. To show this is not the case, we obtain the NESS of the system when adding a staggered local potential

$$H_s = B \sum_{j=1}^{N} (-1)^j n_j \tag{20}$$

that breaks its integrability. For $\gamma = 0$, this has the effect of turning the system into a diffusive conductor in the gapless regime $|\Delta| < 1$ for any driving, while not affecting the existence of NDC at large drivings for $|\Delta| > 1$.[36] In Fig. 13(a), we see that for weak interactions, dephasing monotonically decreases the current, while for strong interactions we confirm, for a variety of field strengths B, that dephasing-enhanced transport occurs, as shown in Fig. 13(b). Thus the existence of NDC and dephasing enhancement, characterizing the nonequilibrium phase transition between weakly and strongly interacting regimes, is independent of integrability. Both effects arise as long as the eigenstructure of the system possesses the features discussed in Secs. IV and V, which for the case considered in this work is valid even if the integrability is broken, as shown in the inset of Fig. 13(b).

From the eigenstructure of the nonintegrable system, the most notable features of the dephasing-enhanced transport can be understood. Namely, the increase of the optimal dephasing rate γ_{opt} with B results from the splitting of the energy bands due to the staggered potential, as shown in Fig. 13(b) [compare to Fig. 6(a)]. This split emerges from different energy shifts of the eigenstates of the system, which depend on their spatial distribution.[64] Due to the band splitting and the emergence of

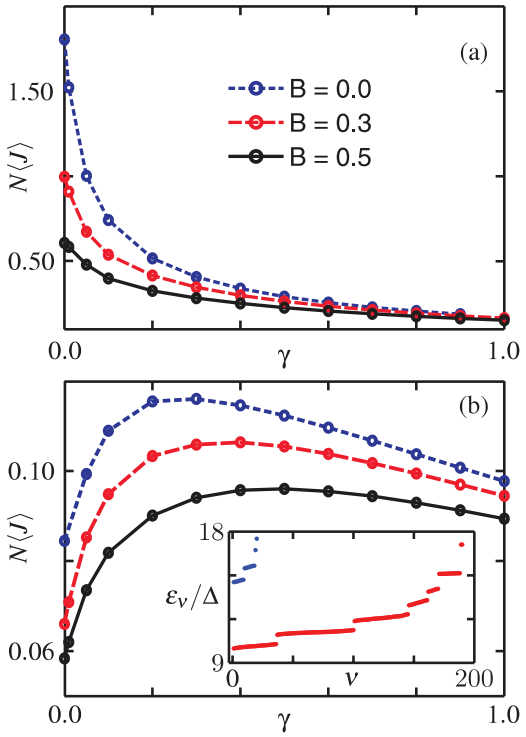

FIG. 13. (Color online) The current through the system for several staggered potential strengths B, for $N = 40$, $f = 0.1$, and $\Gamma = 1$, with (a) $\Delta = 0.5$ and (b) $\Delta = 2.0$. Inset: energy eigenspectrum for one (blue) and two (red) excitations of a chain of $N = 20$, with staggered potential $B = 2$ and interaction $\Delta = 10$.

new energy gaps, the states of wide bands of lowest energy become harder to populate, so a larger energy dissipation is required to induce transitions towards them, and thus to enhance the transport. In addition, note that the staggered potential also flattens all the energy bands, reducing the conductivity through the chain.

VII. CONCLUSIONS

We have presented a detailed study of the effects of dephasing on the transport properties of a boundary driven one-dimensional interacting spinless fermion chain. The appearance of a cooperative many-body NESS exhibiting NDC at strong interactions provides a previously unexplored form of dephasing enhanced transport, distinct in origin from earlier examples in noninteracting systems. Using a toy model for the very strongly interacting regime, we isolated the minimum requirements for observing NDC and dephasing enhanced transport. These consist of the emergence of a gapped eigenstructure with bands of eigenstates possessing different mobility, and the transitions between states of different bands induced by incoherent processes. At maximal driving and no dephasing, approximate dark states are preferentially populated, inducing an insulating steady state. The introduction of dephasing populates mobile bands due to energy dissipation, turning the system into a diffusive conductor. A similar mechanism occurs even in the linear response regime of very large systems, leading to a significant enhancement of the current.

While our discussion of the transport properties has been focused on the NESS of the driven interacting system, it is also highly relevant for transient dynamics. Specifically, since the growth of a particle domain requires the propagation of holes toward the left boundary, the increasing suppression of this process in each successive particle number sector n leads to an exponentially slow convergence to the NESS.[36] The transient current is effectively suppressed even for a small domain $n > 5$ and this is the physical reason why our numerical calculation of the NESS for $f = 1$ is limited to relatively small systems when $\gamma = 0$. As such, the existence of approximate dark states $|\Psi_D(n)\rangle$ at $f = 1$ heavily influences the dynamics far from stationarity and indicates that dephasing enhancement will be significant in the transient regime as well.

For moderate dephasing, the different nature of the NESS at weak and strong interactions was revealed by the emergence of large correlations, and reflects an underlying nonequilibrium phase transition in the system. As such, dephasing enhancement as well as the NDC for $|\Delta| \to 1$ are truly many-body phenomena. A recent study has also observed both NDC and dephasing enhancement of heat transport in the same system with strong interactions.[60] These effects are also unrelated to integrability, suggesting that our findings will also apply to more realistic strongly correlated systems such as the $t - J$ or Hubbard models.

Dephasing enhancement is also expected to be found in nonequilibrium systems with a different transport process. The most important example corresponds to that of the expansion on an initially trapped wave packet.[19,20,63] Tantalizing signs of noise induced breakup of bound states and subsequent increase of the expansion of a strongly interacting packet have already been observed in a recent cold-atom simulation.[18] The general enhancement mechanism predicted in the present work also provides an explanation for this result when applied to this type of transient dynamics. Furthermore, given the recent advances in experiments on transport of ultracold atomic gases, the prospects of verifying more directly both NDC and dephasing enhancement are promising.[33,34]

ACKNOWLEDGMENTS

J.J.M.-A. acknowledges Departamento Administrativo de Ciencia, Tecnología e Innovación Colciencias for economic support. D.J. and S.R.C. thank the National Research Foundation and the Ministry of Education of Singapore for support.

APPENDIX A: EXISTENCE OF AN INSULATING STATE AT $f = 1$ WHEN $|\Delta| \gg 1$

Formally, a dark state $|\psi\rangle$ of an open quantum system is a pure state, which is simultaneously an eigenstate of the Hamiltonian $H|\psi\rangle = E|\psi\rangle$ and a zero-eigenvalue eigenstate of all the jump operators comprising the dissipator $\mathcal{L}(|\psi\rangle\langle\psi|) = 0$ that describes the noise acting on the system. In this section, we show that deep in the strongly interacting limit $|\Delta| \gg 1$, with maximal driving $f = 1$, as indicated in Fig. 14(a), there exists a state $|\Psi_D\rangle$ that, as the system size N grows, becomes exponentially close to satisfying these requirements and is thus an approximate dark state. As described in Sec. IV, the demonstration consists of two parts.

1. Existence of a dark state for maximal driving $f = 1$

As shown in Fig. 6(b), the driving scheme of the strongly interacting limit $|\Delta| \to \infty$ couples the four eigenstates $|0\mathbf{x}0\rangle, |0\mathbf{x}1\rangle, |1\mathbf{x}0\rangle, |1\mathbf{x}1\rangle$, establishing a quadruplet defined by the string $\mathbf{x}$. At $f = 1$, the states $|1\mathbf{x}0\rangle$ become dark, of which the n-particle domain configurations $|B_n\rangle$ play a prominent role. Namely, for finite but large interaction $|\Delta|$, they weakly hybridize with break-away configurations, resulting in the high-energy bound eigenstates $|\Psi_D(n)\rangle$. In Fig. 14(b), the pattern of incoherent driving transitions and coherent hopping for $N = 4$ is illustrated. Note that in this case $|B_2\rangle = |1100\rangle$ has no direct coherent transition to any configurations that couple to the $f = 1$ driving. It only couples to the state $|1010\rangle$, which is also a dark configuration. More generally, so long as $N \geqslant 4$ and $n \geqslant 2$, the break-away configuration for any domain state $|B_n\rangle$ is also a dark configuration of its own quadruplet.

We now compute the high-order corrections to the states $|B_n\rangle$ due to hopping to build a perturbative picture of the bound eigenstates $|\Psi_D(n)\rangle$. Since $|\Delta| \gg 1$, it is instructive to do this approximately by focusing on states describing a single break-away particle or hole propagating away from the domain wall at site n. These have the form $c_j c_k^\dagger |B_n\rangle$, where $1 \leqslant j \leqslant n$ and $n < k \leqslant N$. Since the repeated action of hopping on $|B_n\rangle$ originates around the domain wall, and is also detuned by the gap Δ, we find that hopping mixes in configurations where the particle and/or hole have hopped x times in total, with an amplitude scaling as $O(|2\Delta|^{-x})$. This indicates that the particle/hole propagation through the empty/unit-filled regions is suppressed with its distance from the domain wall. For each n, the eigenstate $|\Psi_D(n)\rangle$ is therefore predicted by this particle-hole (ph) picture to have a domain wall that remains exponentially localized at site n, within a length scale $\xi \sim 1/\ln(|2\Delta|)$,[36] and a deviation $\delta_n(j)$ from the perfect domain configuration $|B_n\rangle$ given by

$$\delta_n^{\mathrm{ph}}(j) = \begin{cases} \left(\frac{1}{|2\Delta|}\right)^{2(n-j+1)}, & 1 \leqslant j \leqslant n, \\ \left(\frac{1}{|2\Delta|}\right)^{2(j-n)}, & n < j \leqslant N. \end{cases} \tag{A1}$$

The validity of this picture is established by comparing this to the actual density deviation $\delta_n(j)$ of the exact eigenstate $|\Psi_D(n)\rangle$. In Fig. 15, this is done for $|\Psi_D(N/2)\rangle$ with $N = 12$ and $\Delta = 10$, and the agreement between $\delta_n(j)$ and $\delta_n^{\mathrm{ph}}(j)$ is seen to be excellent everywhere but the boundaries.

Since hopping predominately connects $|B_n\rangle$ with dark configurations of the form $|1\mathbf{x}0\rangle$, the leading order contribution to the amplitude in $|\Psi_D(n)\rangle$ for a configuration that is not dark is $O(|\Delta|^{-\min(n,|n-N/2|)})$. This corresponds to whether the hole or particle has the shortest path to the left or right boundary, respectively. In the $|\Delta| \gg 1$ limit, we therefore conclude that the eigenstates $|\Psi_D(n)\rangle$, with $0 \leqslant n \leqslant N/2$, form a hierarchy of states with n, characterized by a decreasing amplitude for any configuration to be coupled to the $f = 1$ boundary driving. Eigenstates $|\Psi_D(n)\rangle$ with a domain size n scaling with N thus become exponentially close to being zero eigenstates of the

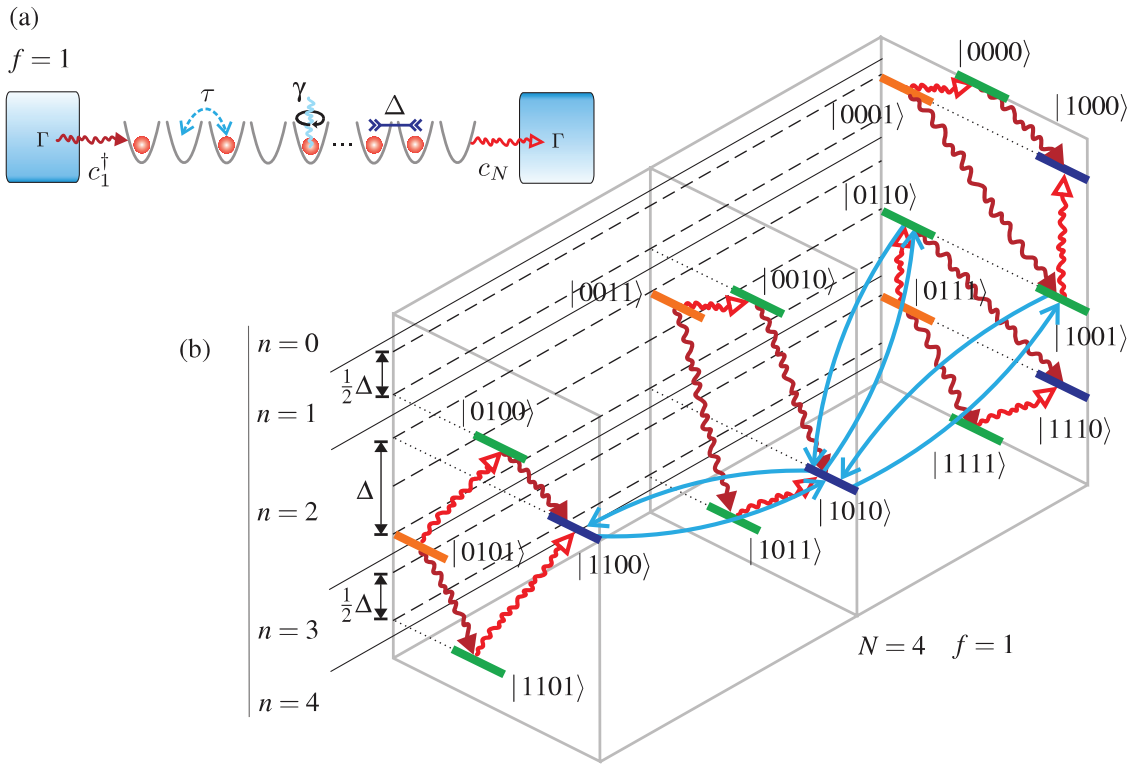

FIG. 14. (Color online) (a) A schematic of the system, showing the coherent hopping τ, the nearest-neighbor density-density interaction Δ, dephasing γ, and the incoherent boundary driving in the strong driving limit $f = 1$ where the bias is maximal. In this case, the driving incoherently pumps particles into the system at site 1 and ejects them at site N, both at a rate Γ. (b) For $N = 4$ sites and $f = 1$, the complete set of driving quadruplets and the transitions induced by coherent hopping between them from the half-filled domain state $|1100\rangle$ is shown. The vertical axis displays the particle number sectors and energy gaps between configurations. We observe that for $N = 4$ one hop connects $|1100\rangle$ to $|1010\rangle$, which is a dark configuration of its quadruplet, and a further hop is needed before it is coherently connected to a configuration that is not dark to the $f = 1$ driving. This disconnection between the half-filled domain configuration and the driving only occurs for $N \geqslant 4$, and so this is the smallest size that displays NDC.

$f = 1$ driving with increasing system size. Of these states, the one with $n = N/2$, where the domain spans exactly half the chain, has the most suppressed coupling $O(|\Delta|^{-N/2})$ to the driving and is thus the closest approximation of all of them

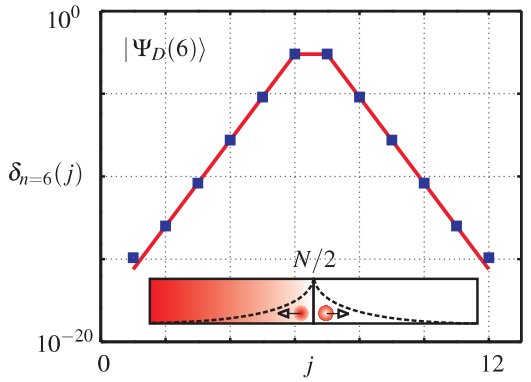

FIG. 15. (Color online) For the eigenstate $|\Psi_D(6)\rangle$ for $N = 12$ and $\Delta = 10$, the exact density deviation $\delta_n(j)$ from the corresponding boundary domain configuration $|B_n\rangle$ is shown (■), along with $\delta_n^{\text{ph}}(j)$ predicted by considering single particle/hole propagation (solid line). The inset shows a schematic of the expected exponential localization of the domain wall.

to an exact dark state. Now we show that this is precisely the state preferentially populated by the driving process.

2. Structure of the NESS in the $|\Delta| \gg 1$ limit

The open dynamics of particle number conserving systems like that considered here have been studied extensively[36,45] with regard to their ergodic and mixing properties, and it has been established that a unique NESS exists for any f. The key property ensuring this is that for a finite hopping amplitude every configuration within each particle number sector can be reached from any other, while the incoherent ejection/injection of particles by the driving connects neighboring sectors. As a result, the complete state space of the system can be accessed. Furthermore, the NESS for this open system will be block diagonal in the number sectors. At $f = 1$, the approximate dark states $|\Psi_D(n)\rangle$ for each sector n are expected to play a prominent role due to their ability to trap population. This can be better understood by approximating the NESS as a statistical mixture, with probabilities p_n, of these eigenstates in each sector as

$$\rho = \sum_{n=0}^{N} p_n |\Psi_D(n)\rangle\langle\Psi_D(n)|. \tag{A2}$$

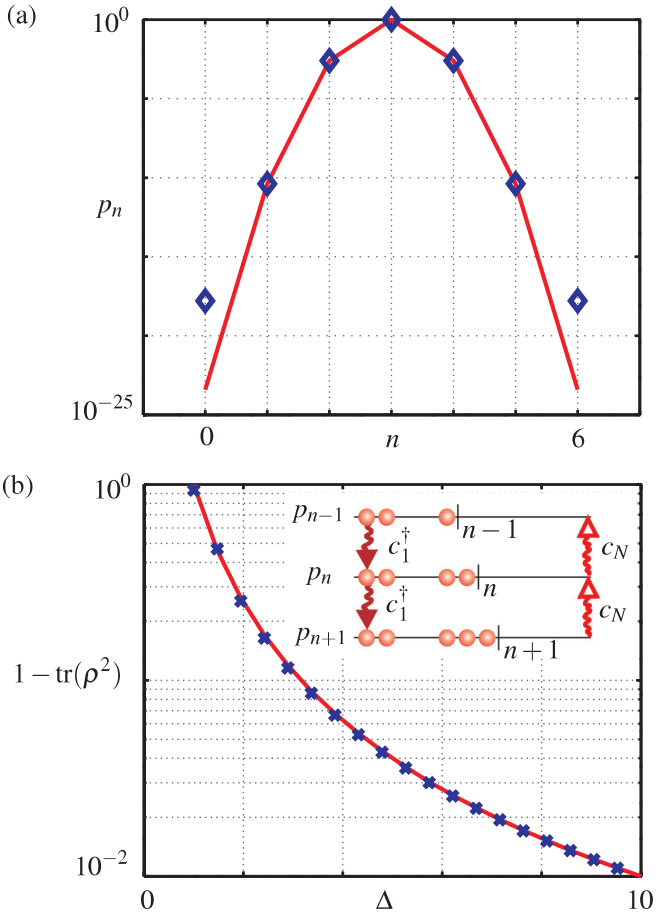

FIG. 16. (Color online) (a) The probability p_n on a logarithmic scale of the NESS ρ occupying the n particle sector is shown for an exact calculation ($\diamond$) for $N = 6$ and $\Delta = 10$, and the predicted form (solid line) given in Eq. (A4). (b) The purity $1 - \mathrm{tr}(\rho^2)$ against Δ of the NESS ρ on a logarithmic scale for an exact calculation ($\times$) for $N = 6$ and the predicted form (solid line) given in Eq. (A5). The inset shows a schematic of the detailed balance approximation applied to compute these predictions.

The purity of the NESS in this approximation, $\mathrm{tr}(\rho^2) = \sum_{n=0}^{N} p_n^2$, is reduced only through mixing between sectors. The probabilities p_n are then determined by demanding that at stationarity there is a detailed balance condition between the incoherent transition rates connecting neighboring number sectors [see inset of Fig. 16(b)]. For sector n, assumed to be frozen in the state $|\Psi_D(n)\rangle$, the output transition rates scale with the probability of a hole being at the left boundary as $\Gamma\langle\Psi_D(n)|c_1 c_1^\dagger|\Psi_D(n)\rangle \sim \Gamma|2\Delta|^{-2n}$, and the probability of a particle being at the right boundary as $\Gamma\langle\Psi_D(n)|c_N^\dagger c_N|\Psi_D(n)\rangle \sim \Gamma|2\Delta|^{-2(N-n)}$. Considering sectors $n-1$, n and $n+1$ we then have the equality of incoming and outgoing transitions in n as

$$p_n\left[\left(\frac{1}{|2\Delta|}\right)^{2n} + \left(\frac{1}{|2\Delta|}\right)^{2(N-n)}\right] = p_{n-1}\left(\frac{1}{|2\Delta|}\right)^{2(n-1)} + p_{n+1}\left(\frac{1}{|2\Delta|}\right)^{2(N-n-1)}. \quad \text{(A3)}$$

These equations are solved inwards from the extremal $n = 0$ and $n = N$ sectors, where $|\Psi_D(0)\rangle = |00\ldots00\rangle$ and $|\Psi_D(N)\rangle = |11\ldots11\rangle$, to give

$$p_n = p\left(\frac{1}{|2\Delta|}\right)^{2|n-N/2|^2}, \quad \text{(A4)}$$

for $n = 0, 1, \ldots, N$ and where $p = p_{N/2}$ is fixed by the normalization condition $\sum_{n=0}^{N} p_n = 1$. In Fig. 16(a), these predicted probabilities of occupation for each sector n are plotted against the exact values for the NESS with $N = 6$ and $\Delta = 10$ and found to yield excellent agreement aside from the extremal sectors. Owing to the hierarchy of approximate dark states, this indicates that the NESS will be predominately a mixture of $|\Psi_D(n)\rangle$ peaked around the "best" dark state with $n = N/2$. This result also predicts that to lowest order in $|\Delta|^{-1}$, the purity of ρ is given by

$$\mathrm{tr}(\rho^2) \approx p_{N/2}^2 \approx 1 - \frac{1}{|\Delta|^2} + \cdots, \quad \text{(A5)}$$

which is independent of the size of the system. In Fig. 16(b), this prediction is plotted against the exact value of $1 - \mathrm{tr}(\rho^2)$ of the NESS for $N = 6$ as a function of Δ, again showing excellent agreement even as $\Delta \to 1$.

APPENDIX B: EQUIVALENCE OF DEPHASING AND DRIVING EFFECTS IN THE TOY MODEL AT LARGE DRIVING

The correspondence between a slight increase of dephasing from zero and a slight decrease of the driving f from unity, indicated in Eq. (16), is confirmed in Fig. 17(a) in an exact calculation for the toy model with $K = 20$. This equivalence is understood by considering the mean backward flow process introduced when driving slightly below $f = 1$. In this limit, the rate of driving from $|K\rangle \to |s\rangle$ taking the state out of $|\Psi_D\rangle$ is given by $\frac{1}{2}(1-f)\Gamma$ and therefore slow. In contrast the rate of driving $|s\rangle \to |K\rangle$ back is $\frac{1}{2}(1+f)\Gamma$, and therefore rapid. Focusing on the dynamics of these two driving processes

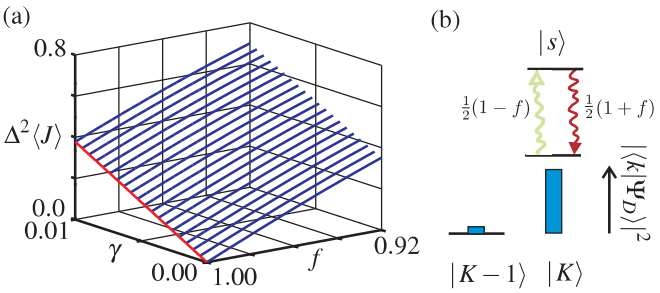

FIG. 17. (Color online) (a) The NESS current $\langle J\rangle$, rescaled by Δ^2, for $K = 20$ is shown as a function of the driving f and dephasing γ zoomed in around the limit $f = 1$, $\gamma = 0$ insulating point [see Fig. 8(a)]. The behavior at $f = 1$ with γ is emphasized by the additional (red) line. (b) In the strong driving limit $f \sim 1$, the Λ_R^- process $|K\rangle \to |s\rangle$ occurs at a rate $\propto (1-f) \ll 1$ making it slow (as indicated by being faded out), while the Λ_R^+ process $|s\rangle \to |K\rangle$ occurs at a rate $\propto f \approx 1$ and so is rapid. The dominant driving process is therefore $|K\rangle \to |s\rangle \to |K\rangle$, which has the effect of destroying any coherence $|K\rangle$ has with other states, such as $|K-1\rangle$.

alone, as in Fig. 17(b), we suppose that the initial state of the system over the configurations $|s\rangle, |K-1\rangle$, and $|K\rangle$ has the form

$$\rho(0) = \begin{pmatrix} 0 & 0 & 0 \\ 0 & \rho_{K-1}(0) & \rho_{K-1,K}(0) \\ 0 & \rho^*_{K-1,K}(0) & \rho_K(0) \end{pmatrix}, \tag{B1}$$

where there is some coherence between $|K-1\rangle$ and $|K\rangle$, but no population initially in $|s\rangle$. Evolving this state according only to these driving processes yields solutions

$$\begin{aligned} \rho_s(t) &= \tfrac{1}{2}(1-f)\Gamma(1-e^{-\Gamma t})\rho_K(0), \\ \rho_K(t) &= e^{-\Gamma t}\rho_K(0) + \tfrac{1}{2}(1+f)\Gamma(1-e^{-\Gamma t})\rho_K(0), \\ \rho_{K-1}(t) &= \rho_{K-1}(0), \\ \rho_{K-1,K}(t) &= e^{-\frac{1}{4}(1-f)\Gamma t}\rho_{K-1,K}(0). \end{aligned} \tag{B2}$$

We therefore find that for the populations, the stationary $t \to \infty$ limit is approached at a rate Γ to give

$$\begin{aligned} \rho_s(\infty) &= \tfrac{1}{2}(1-f)\Gamma\rho_K(0), \\ \rho_K(\infty) &= \tfrac{1}{2}(1+f)\Gamma\rho_K(0), \end{aligned} \tag{B3}$$

while the coherence $\rho_{K-1,K}(t)$ decays exponentially to zero at a rate $\frac{1}{4}(1-f)\Gamma$. Now, by considering only the dephasing process, we instead find that the populations are unchanged while the coherence decays as

$$\rho_{K-1,K}(t) = e^{-2\gamma t}\rho_{K-1,K}(0). \tag{B4}$$

Matching of these decoherence rates again yields Eq. (16). We therefore conclude that the emergence of a nonzero current when reducing f from unity is, to leading order, caused by the resulting decoherence of the dark state $|\Psi_D\rangle$, identical to the effect of dephasing alone. This behavior with f around $f = 1$, combined with $\langle J\rangle = 0$ at $f = 0$ and the continuity of $\langle J\rangle$ with f, is already enough to imply that NDC behavior will be observed in the current-driving profile. Thus NDC and dephasing enhancement are underpinned by the same mechanism.

[1] G. S. Engel, T. R. Calhoun, E. L. Read, T.-K. Ahn, T. Mancal, Y.-C. Cheng, R. E. Blankenship, and G. R. Fleming, Nature (London) **446**, 782 (2007).

[2] H. Lee, Y.-C. Cheng, and G. R. Fleming, Science **316**, 1462 (2007).

[3] E. Collini, C. Y. Wong, K. E. Wilk, P. M. G. Curmi, P. Brumer, and G. D. Scholes, Nature (London) **463**, 644 (2010).

[4] M. Mohseni, P. Rebentrost, S. Lloyd, and A. Aspuru-Guzik, J. Chem. Phys. **129**, 174106 (2008).

[5] M. B. Plenio and S. F. Huelga, New J. Phys. **10**, 113019 (2008).

[6] F. Caruso, A. W. Chin, A. Datta, S. F. Huelga, and M. B. Plenio, J. Chem. Phys. **131**, 105106 (2009).

[7] P. Rebentrost, M. Mohseni, I. Kassal, S. Lloyd, and A. Aspuru-Guzik, New J. Phys. **11**, 033003 (2009).

[8] A. W. Chin, A. Datta, F. Caruso, S. F. Huelga, and M. B. Plenio, New. J. Phys. **12**, 065002 (2010).

[9] A. Olaya-Castro, C. F. Lee, F. F. Olsen, and N. F. Johnson, Phys. Rev. B **78**, 085115 (2008).

[10] D. Manzano, PLoS One **8**, e57041 (2013).

[11] F. Caruso, N. Spagnolo, C. Vitelli, F. Sciarrino, and M. B. Plenio, Phys. Rev. A **83**, 013811 (2011).

[12] D. Manzano, M. Tiersch, A. Asadian, and H. J. Briegel, Phys. Rev. E **86**, 061118 (2012).

[13] F. Caruso, S. F. Huelga, and M. B. Plenio, Phys. Rev. Lett. **105**, 190501 (2010).

[14] A. Bermudez, T. Schaetz, and M. B. Plenio, Phys. Rev. Lett. **110**, 110502 (2013).

[15] D. Poletti, P. Barmettler, A. Georges, and C. Kollath, arXiv:1212.4637.

[16] D. Poletti, J.-S. Bernier, A. Georges, and C. Kollath, Phys. Rev. Lett. **109**, 045302 (2012).

[17] D. Poletti, J.-S. Bernier, A. Georges, and C. Kollath, arXiv:1212.4254.

[18] C. D'Errico, M. Moratti, E. Lucioni, L. Tanzi, B. Deissler, M. Inguscio, G. Modugno, M. B. Plenio, and F. Caruso, New J. Phys. **15**, 045007 (2013).

[19] D. Gobert, C. Kollath, U. Schollwöck, and G. Schütz, Phys. Rev. E **71**, 036102 (2005).

[20] S. Langer, F. Heidrich-Meisner, J. Gemmer, I. P. McCulloch, and U. Schollwöck, Phys. Rev. B **79**, 214409 (2009).

[21] S. Keßler, A. Holzner, I. P. McCulloch, J. von Delft, and F. Marquardt, Phys. Rev. A **85**, 011605(R) (2012).

[22] A. V. Sologubenko, T. Lorenz, H. R. Ott, and A. Freimuth, J. Low Temp. Phys. **147**, 387 (2007).

[23] F. Heidrich-Meisner, A. Honecker, and W. Brenig, Eur. Phys. J. Special Topics **151**, 135 (2007).

[24] N. Hlubek, P. Ribeiro, R. Saint-Martin, A. Revcolevschi, G. Roth, G. Behr, B. Büchner, and C. Hess, Phys. Rev. B **81**, 020405(R) (2010).

[25] O. Janson, A. A. Tsirlin, and H. Rosner, Phys. Rev. B **82**, 184410 (2010).

[26] R. Hanson, L. P. Kouwenhoven, J. R. Petta, S. Tarucha, and L. M. K. Vandersypen, Rev. Mod. Phys. **79**, 1217 (2007).

[27] J. C. Cuevas and E. Scheer, *Molecular Electronics: An introduction to Theory and Experiment* (World Scientific, Singapore, 2010).

[28] J. T. Barreiro, M. Müller, P. Schindler, D. Nigg, T. Monz, M. Chwalla, M. Hennrich, C. F. Roos, P. Zoller, and R. Blatt, Nature (London) **470**, 486 (2011).

[29] A. Kay and D. G. Angelakis, Europhys. Lett. **84**, 20001 (2008).

[30] S. Trotzky, P. Cheinet, S. Fölling, M. Feld, U. Schnorrberger, A. M. Rey, A. Polkovnikov, E. A. Demler, M. D. Lukin, and I. Bloch, Science **319**, 295 (2008).

[31] J. Simon, W. S. Bakr, R. Ma, M. E. Tai, P. M. Preiss, and M. Greiner, Nature (London) **472**, 307 (2011).

[32] J. P. Ronzheimer, M. Schreiber, S. Braun, S. S. Hodgman, S. Langer, I. P. McCulloch, F. Heidrich-Meisner, I. Bloch, and U. Schneider, Phys. Rev. Lett. **110**, 205301 (2013).

[33] J.-P. Brantut, J. Meineke, D. Stadler, S. Krinner, and T. Esslinger, Science **337**, 1069 (2012).

[34] D. Stadler, S. Krinner, J. Meineke, J.-P. Brantut, and T. Esslinger, Nature (London) **491**, 736 (2012).

[35]G. Benenti, G. Casati, T. Prosen, and D. Rossini, Europhys. Lett. **85**, 37001 (2009).
[36]G. Benenti, G. Casati, T. Prosen, D. Rossini and M. Žnidarič, Phys. Rev. B **80**, 035110 (2009).
[37]T. Prosen, Phys. Rev. Lett. **106**, 217206 (2011).
[38]M. Žnidarič, Phys. Rev. Lett. **106**, 220601 (2011).
[39]M. Žnidarič, New J. Phys. **12**, 043001 (2010).
[40]I. Kassal and A. Aspuru-Guzik, New J. Phys. **14**, 053041 (2012).
[41]H.-P. Breuer and F. Petruccione, *The Theory of Open Quantum Systems* (Oxford University Press, Oxford, 2002).
[42]The validity of the master equation description in this regime was established in earlier works.[35–38]
[43]B. Derrida, Phys. Rep. **301**, 65 (1998).
[44]O. Golinelli and K. Mallick, J. Phys. A **39**, 12679 (2006).
[45]D. Burgarth and V. Giovannetti, Phys. Rev. Lett. **99**, 100501 (2007).
[46]M. Zwolak and G. Vidal, Phys. Rev. Lett. **93**, 207205 (2004).
[47]F. Verstraete, J. J. García-Ripoll, and J. I. Cirac, Phys. Rev. Lett. **93**, 207204 (2004).
[48]M. Michel, O. Hess, H. Wichterich, and J. Gemmer, Phys. Rev. B **77**, 104303 (2008).
[49]J. Wu and M. Berciu, Phys. Rev. B **83**, 214416 (2011).
[50]V. Popkov, M. Salerno, and G. M. Schütz, Phys. Rev. E **85**, 031137 (2012).
[51]S. Al-Assam, S. R. Clark, and D. Jaksch and TNT Development Team, TNT Library alpha version (2012), http://www.tensornetworktheory.org.
[52]T. Prosen and M. Žnidarič, J. Stat. Mech. (2009) P02035.
[53]M. Žnidarič, J. Stat. Mech. (2010) L05002.
[54]X. Zotos, F. Naef, and P. Prelovšek, Phys. Rev. B **55**, 11029 (1997).
[55]T. Prosen, Phys. Rev. Lett. **107**, 137201 (2011).
[56]M. Žnidarič, Phys. Rev. E **83**, 011108 (2011).
[57]D. J. Griffiths, *Introduction to Quantum Mechanics*, 2nd ed. (Pearson Education, Upper Saddle River, New Jersey, 2005).
[58]B. Sutherland, *Beautiful Models. 70 Years of Exactly Solved Quantum Many-Body Problems* (World Scientific, Singapore, 2005).
[59]M. Takahashi, *Thermodynamics of One-Dimensional Solvable Models* (Cambridge University Press, Cambridge, UK, 1999).
[60]J. J. Mendoza-Arenas, S. Al-Assam, S. R. Clark, and D. Jaksch, arXiv:1303.6353.
[61]M. Žnidarič, T. Prosen and I. Pižorn, Phys. Rev. A **78**, 022103 (2008).
[62]T. Prosen and M. Žnidarič, Phys. Rev. Lett. **105**, 060603 (2010).
[63]S. Jesenko and M. Žnidarič, Phys. Rev. B **84**, 174438 (2011).
[64]The simplest case illustrating this point is that of one excitation in an even chain with $\Delta \to \infty$; if $B = 0$ the states $|10\cdots0\rangle$ and $|0\cdots01\rangle$ are degenerate, while if $B > 0$, they experience negative and positive energy shifts, respectively.